

## Video Article

# A Comprehensive Protocol for Manual Segmentation of the Medial Temporal Lobe Structures

Matthew Moore\*<sup>1</sup>, Yifan Hu\*<sup>1</sup>, Sarah Woo<sup>1</sup>, Dylan O'Hearn<sup>1</sup>, Alexandru D. Iordan<sup>2,3</sup>, Sanda Dolcos<sup>1</sup>, Florin Dolcos<sup>1,2,3</sup><sup>1</sup>Psychology Department, University of Illinois Urbana-Champaign<sup>2</sup>Neuroscience Program, University of Illinois Urbana-Champaign<sup>3</sup>Beckman Institute for Advanced Science and Technology, University of Illinois Urbana-Champaign

\*These authors contributed equally

Correspondence to: Florin Dolcos at [fdolcos@illinois.edu](mailto:fdolcos@illinois.edu)URL: <http://www.jove.com/video/50991>DOI: [doi:10.3791/50991](https://doi.org/10.3791/50991)

Keywords: Neuroscience, Issue 89, Anatomy, Segmentation, Medial Temporal Lobe, MRI, Manual Tracing, Amygdala, Hippocampus, Perirhinal Cortex, Entorhinal Cortex, Parahippocampal Cortex

Date Published: 7/2/2014

Citation: Moore, M., Hu, Y., Woo, S., O'Hearn, D., Iordan, A.D., Dolcos, S., Dolcos, F. A Comprehensive Protocol for Manual Segmentation of the Medial Temporal Lobe Structures. *J. Vis. Exp.* (89), e50991, doi:10.3791/50991 (2014).

## Abstract

The present paper describes a comprehensive protocol for manual tracing of the set of brain regions comprising the medial temporal lobe (MTL): amygdala, hippocampus, and the associated parahippocampal regions (perirhinal, entorhinal, and parahippocampal proper). Unlike most other tracing protocols available, typically focusing on certain MTL areas (e.g., amygdala and/or hippocampus), the integrative perspective adopted by the present tracing guidelines allows for clear localization of all MTL subregions. By integrating information from a variety of sources, including extant tracing protocols separately targeting various MTL structures, histological reports, and brain atlases, and with the complement of illustrative visual materials, the present protocol provides an accurate, intuitive, and convenient guide for understanding the MTL anatomy. The need for such tracing guidelines is also emphasized by illustrating possible differences between automatic and manual segmentation protocols. This knowledge can be applied toward research involving not only structural MRI investigations but also structural-functional colocalization and fMRI signal extraction from anatomically defined ROIs, in healthy and clinical groups alike.

## Video Link

The video component of this article can be found at <http://www.jove.com/video/50991/>

## Introduction

The medial temporal lobe (MTL), a putative area of the highest level of integration of sensory information<sup>1</sup>, has been a frequent subject of targeted analyses. For example, the hippocampus and the associated parahippocampal areas have been extensively studied in memory research<sup>2-5</sup>. Also, the role of the amygdala has been frequently emphasized in research examining emotion processing and emotion-cognition interactions<sup>6-11</sup>. Recently, various MTL regions have also received attention in the emerging field of personality neuroscience, which links the structure and function of these and other brain regions to individual variation in personality traits<sup>12</sup>. Assessing the anatomy and function of the MTL structures can be important in facilitating diagnosis of degenerative diseases where specific structural and functional anomalies can occur in different MTL structures. For example, in Alzheimer's disease (AD), significant atrophy of the entorhinal cortex and hippocampus can be observed<sup>13,14</sup>, and atrophy of the hippocampus can predict the transition from mild cognitive impairment to AD<sup>15</sup>. Automatic segmentation algorithms have recently become popular for segmenting cortical and subcortical structures, but as with any tool, these programs inevitably encounter errors in some cases. In such instances a researcher should be equipped with both the knowledge and guidelines to recognize the anatomical borders of the MTL structures. The tendency in the extant literature has been to target individual MTL subregions<sup>16-21</sup>, with many protocols tending to focus on hippocampus<sup>16-19</sup>.

Unlike most of the available published guidelines for MTL tracing, the present protocol provides a comprehensive set of guidelines that allow for clear localization of all MTL subregions. Tracing guidelines for the following MTL structures are described: the amygdala (AMY), the hippocampus (HC), the perirhinal cortex (PRC), the entorhinal cortex (ERC), and the parahippocampal cortex (PHC). The AMY and the HC are traced first, and are then followed by the parahippocampal gyri (PHG) structures. Note that the generic term *HC* is used here to refer to the HC formation, which encompasses the HC proper, the subiculum, and the posterior segment of the uncus<sup>22-24</sup>. Also, note that the PHG can be divided into two segments, the anterior portion and the posterior portion. Within the anterior portion of the PHG, it can be further divided into the lateral and medial anterior PHG, whose cortical areas correspond to the PRC and the ERC, respectively. The PHC, the cortical area of the posterior portion of the PHG, corresponds to the parahippocampal cortex proper. For simplicity reasons, we will be using the terms *PRC* and *ERC* to refer to the lateral and medial anterior PHG, and *PHC* to refer to the posterior PHG. The segmentation for each structure begins with a rough localization of the anterior and posterior borders, along with other relevant landmarks, which is then followed by the actual tracing

performed slice-by-slice in the coronal plane, in an anterior-posterior/rostral-caudal direction. In all cases, the sagittal and axial sections are closely monitored to assist the localization of anatomical boundaries and landmarks.

The need for such tracing guidelines is also illustrated in figures displaying possible differences between the output of automatic and manual segmentation protocols. The advantage of a protocol that describes all of the MTL structures in the current visual format is that variations in the anatomy (e.g., the collateral sulcus [CS] depth) that can affect border definitions can be described in context with the surrounding anatomy (e.g., the PRC and ERC medial and lateral borders vary in location depending on the depth of the CS<sup>25</sup>). This might not be clear or understandable to an inexperienced tracer or an experienced tracer who only traces single or separate structures, and to our knowledge, such a visually comprehensive guideline does not exist.

The present protocol is an explicit presentation of guidelines used for MTL tracing in a previous investigation identifying differential contributions from MTL subregions to the memory enhancing effect of emotion<sup>26</sup>, adapted to higher resolution brain images allowed by recent developments in structural magnetic resonance (MR) imaging. The tracing is illustrated on scans obtained from a healthy volunteer (female, aged 24), using a 3T MR scanner. Anatomical images were acquired as 3D MPRAGE (TR = 1,800 msec; TE = 2.26 msec; FOV = 256 x 256 mm; voxel size = 1 x 0.5 x 0.5 mm) with an acquisition angle parallel to AC-PC. If image data is acquired with a different acquisition angle, such as oblique orientation, the data should be regridded to a parallel or perpendicular orientation to AC-PC, such that anatomical landmark descriptions translate appropriately. The images were then translated to NIFTI format and input into segmentation software<sup>27</sup> for manual tracing. Scan data used in the current protocol was collected as part of a study that was approved by the Institutional Review Board, and the volunteer provided written consent.

By drawing information from various separate tracing protocols for these structures<sup>18-22,25,28-31</sup>, as well as from anatomical analyses and atlases<sup>23,32-37</sup>, the present protocol presents a comprehensive set of guidelines that address inconsistencies in the extant literature. Complemented by the accompanying visual materials, this work is expected to promote clearer understanding of the MTL structures, and stir up interest of future research in adopting manual segmentation, either as a primary method of MTL tracing or as a supplementary method to automatic segmentation. By providing an accurate, intuitive, and convenient guide for understanding the MTL anatomy, this protocol will help researchers identify the location of all MTL subregions, relative to their neighboring structures, even when only some MTL structures are specifically targeted for analyses. This will not only increase localization accuracy but will also help tracers make informed decisions in cases of morphological variation, which is highly likely in the MTL. These guidelines can be applied to research involving structural and/or functional MRI investigations of the MTL, including volumetric analyses and brain anomaly detection, as well as localizing procedures for functional, anatomical, and tractographic analyses, in healthy groups. The present protocol could also be used to inform segmentation of MTL structures for patients (e.g., patients with atrophy), if the major anatomical landmarks are relatively preserved. Tracing clinical subjects' data can take additional time and effort, depending on the severity of atrophy and/or anatomical changes.

It is important to consider the distinction between gyri and cortices when defining ROI. Anatomically, gyrus here refers to both white matter and grey matter, while cortex refers to grey matter only. Depending on the intended use of the ROI, segmentations might include white matter or exclude it.

We recommend the tracing to be performed sequentially, substructure by substructure, one hemisphere at a time. Certain software packages<sup>27</sup> allow for tracing borders outlined on one slice to be pasted onto subsequent slices, a feature that speeds up the process. It is always advisable to reference the opposing hemisphere as needed, in order to check for consistency across the two sides (e.g., in detecting anatomical landmarks). Alternatively, parallel tracing of the same structures within the two hemispheres can also be performed. Regardless of whether the tracing is sequential or parallel, once the process is complete, the tracers should double-check the end-result and make adjustments as needed, referencing both hemispheres and multiple plane views. Depending on the experience of the tracer and the resolution of the imaging data, manual segmentation of the MTL for healthy subject data can take from 8-10 hr or more, in the case of a novice tracer, to 3-4 hr, in the case of an experienced one.

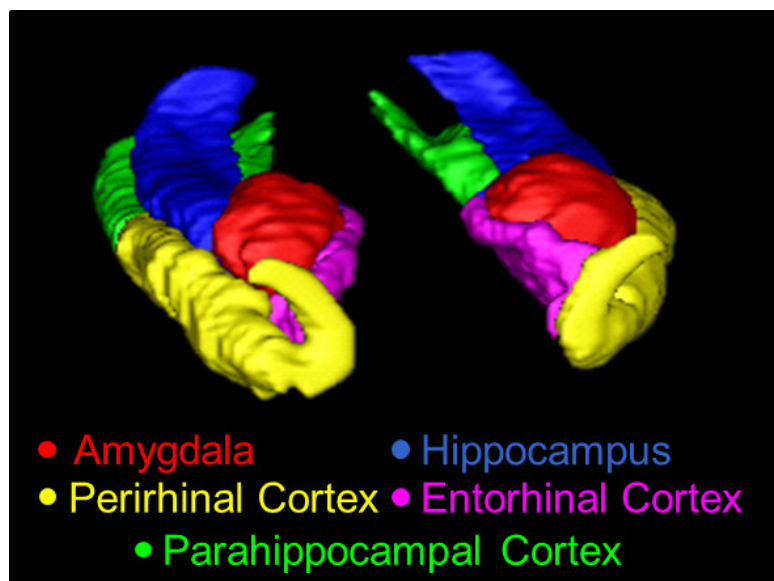


**Figure 1. A 3D overview of the MTL, traced using the present protocol.** Structures shown here are the AMY (red), the HC (blue), the PRC (yellow), the ERC (pink), and the PHC (green).

## Protocol

### 1. Amygdala

1. Anterior Slices of the AMY
  1. Identify the first slice of the AMY in which the limen insula initially appears, where the white matter connection between the frontal and temporal lobes is continuous and visible<sup>30</sup>. In the coronal view, use the angular bundle as the inferolateral border of the AMY.
  2. Locate the optic chiasm as a landmark for the appearance of the AMY. Use the axial and sagittal views to distinguish the AMY in its early slices from the surrounding uncus. Follow the white matter tract around the AMY in the axial view to exclude the entorhinal area<sup>32</sup>.
  3. Moving posteriorly, identify the first slice in which the anterior commissure is continuous throughout both hemispheres<sup>20</sup>, where the AMY is visible in its typical shape. Trace the AMY counter-clockwise using the entorhinal sulcus as the superomedial border, the imaginary line from the fundus of the semianular sulcus along the white matter to the inferior tip of the AMY as the inferomedial border, the temporal stem as the lateral border, and back to the entorhinal sulcus to complete the tracing<sup>31</sup>.
2. Posterior Slices of the AMY
  1. Note that at this level, both the AMY and HC are visible in the same slice(s).
  2. Still in the coronal view, identify the last slice of the AMY where the structure is superior to the medial extension of the temporal horn of lateral ventricle<sup>38</sup> (or the alveus if the ventricle is not present) and lateral to the uncinate gyrus, the protuberance of the head of the HC. Check the sagittal and axial views for accurate and consistent tracing.
  3. Draw an imaginary line from the fundus of the inferior circular sulcus of the insula to the optic tract as the superior border of the AMY<sup>31</sup>, which also differentiates it from the grey matter of the globus pallidus and the putamen.
  4. Trace along the semilunar gyrus as the superomedial border and exclude the uncinate gyrus<sup>32</sup>. Use the inferior horn of the lateral ventricle and the temporal stem for the lateral delineation.
3. Consecutive Slices of the AMY in Anterior-posterior Direction
  1. Systematically trace the AMY slice-by-slice using the relevant guidelines above. At the anterior portion of the AMY, use the same boundaries as for the anterior-most slice; conversely, at the posterior portion of the AMY, use the same boundaries as for the posterior-most slice.
  2. Continue to employ the axial and sagittal views to help define and further refine the AMY borders.

### 2. Hippocampus

1. Localizing the HC
  1. Begin tracing the HC when the temporal horn of the lateral ventricle appears along the inferolateral border of the AMY. If the temporal horn of the lateral ventricle is already present on previous slices, note that the onset of the HC is then indicated by the temporal horn of the lateral ventricle enlarging and stretching superolaterally.
  2. End the tracing of the HC with its last appearance inferomedial to the trigone of the lateral ventricle<sup>31</sup>. Always utilize the alternative views to help localize the HC and its borders.
2. Border Definitions of the HC
  1. Delineate the lateral HC against the temporal horn. In cases where the temporal horn of the lateral ventricle is not perceivable enough, exclude one row of voxels from the segmentation to denote it.
  2. Inferiorly, use the angular bundle (or its imaginary extension) to the ventricular cavity to separate the HC from the PHG. Use the alveus along with the fimbria as the superior border. Trace the HC using the same definitions throughout.
  3. Additionally, include the subiculum into the segmentation such that it medially borders the white matter bundle of the PHG, superiorly aligns with the curve of the uncus, and extends primarily horizontally from the HC<sup>39</sup>. Tracing posteriorly, maintain these definitions until the calcarine sulcus intervenes.
3. Noting Divisions of the HC
  1. Note that the HC can be divided into three segments: head, body, and tail.
  2. Use the appearance of the uncus to mark the transition from the HC head to the HC body, and the rapid ascending and expansion in size, which typically coincides with the appearance of the crus of the fornix, to signify the appearance of the HC tail<sup>23,30,40</sup>.
4. Pay special attention when tracing the following structures.
  1. Include the posterior uncus in the segmentation.
  2. Omit the choroid plexus above the alveus from the segmentation on the coronal slices, although this may not be possible on lower-resolution images.
  3. Refer to the two alternative views to avoid the inclusion of the tail of the caudate and the pulvinar at the superior aspect of the HC tail.
  4. Avoid inclusion of the fascicular gyrus by noting its emergence at the level of the crus of the fornix, where initially it is separated from the hippocampal tail by the fasciola cinerea and more posteriorly becomes the grey matter superior to the calcarine sulcus<sup>32</sup>.

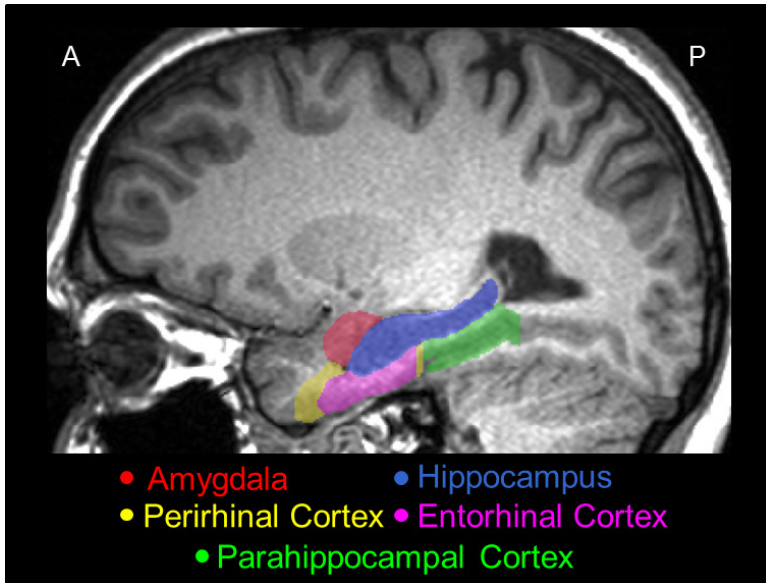


Figure 2. A representative sagittal slice of the MTL traced using the present protocol, showing its actual position in the brain, and the relative positions among its major structures, *i.e.*, the AMY (red), the HC (blue), the PRC (yellow), the ERC (pink), and the PHC (green).

### 3. Parahippocampal Gyrus

1. Noting Divisions of the PHG
  1. Note that the PHG can be divided into two main segments: the anterior PHG (*i.e.*, the PRC and ERC), and the posterior PHG (*i.e.*, the PHC).
  2. Note that in the anterior segment, the PRC appears earlier than the ERC, and flanks it laterally through its entire course.
  3. After the ERC disappears, note that the PRC subsumes its place on the PHG and continues on for 3 mm.
  4. Beyond this segment, trace the posterior PHG, where the PHC takes over the width of the PHG until its end<sup>30</sup>.
2. Anterior Slices of the PHG
  1. Define the first slice of the PRC with the appearance of the CS<sup>25,34</sup>. Before the onset of the ERC, trace the PRC from the medial edge of the lateral bank of the CS to the lateral fundus of the gyrus of Schwalbe, or that of the medial one if two gyri of Schwalbe are present, or the midpoint of the dorsal temporopolar surface in the absence of this gyrus<sup>25,34</sup>.
  2. Start to trace the ERC 5 mm anterior to the limen insula<sup>35,36</sup>.
  3. Continue tracing the ERC using the fundus of the medial temporopolar sulcus as the superior end<sup>35</sup>, and the fundus of the semiannular sulcus after the AMY appears, or the point where the imaginary extension of the angular bundle meets the ventricular cavity if the semiannular sulcus is indistinguishable<sup>25</sup>. Note that it extends inferiorly to meet the ventricular cavity or the pial surface directly.
  4. The border between the PRC and the ERC may vary from slice to slice.
    1. When the CS is *deep* ( $\geq 1.5$  cm), trace the PRC from the medial edge of the medial bank of this sulcus, to the midpoint of its lateral bank<sup>25</sup>.
    2. In cases with a *regular* CS (depth of 1–1.5 cm), trace the PRC as the area from the midpoint of the medial bank of the collateral sulcus to the medial end of the lateral bank of the sulcus<sup>25</sup>.
    3. With a *shallow* CS ( $< 1$  cm), trace the PRC from the fundus of this sulcus to the midpoint of the crown of the fusiform gyrus<sup>25</sup>.
  5. When the CS is interrupted, usually at the level of the uncus apex, by a small gyrus emerging from its fundus, trace the PRC to the fundus of the lateral sulcus<sup>25</sup>. Include or exclude white matter according to the goal for the ROI.
  6. Trace the ERC until 1.5 mm posterior to the uncus apex, or the end of the gyrus intralimbicus<sup>37</sup>.
  7. Extend the tracing of the PRC medially to occupy the place of the ERC after its termination, where the definitions for the latter continue to apply until 4.5 mm posterior to the uncus apex, or the end of the gyrus intralimbicus<sup>37</sup>. The PRC is then substituted by the PHC<sup>25,30</sup>.
3. Posterior Slices of the PHG
  1. Start to trace the PHC on the slice posterior to the end of the PRC, until 4 mm posterior to the end of the HC tail<sup>32</sup>. Alternative definitions from the literature are described in the Discussion section. Again, include or exclude white matter depending on the goal.
  2. Delineate the PHC using the same method described in the posterior portion of the PRC after the disappearance of the ERC. Also use the white matter of the cingulum as the superior border once it appears. Continue tracing in this fashion until the appearance of the calcarine sulcus, which restricts the PHC superomedially to the inferior edge of the sulcus<sup>30</sup>.
  3. Should a mini-sulcus appear before the emergence of the calcarine sulcus, include it in the segmentation, but be cautious in differentiating it from the calcarine sulcus.

Representative Results

Illustration of Possible Differences between Manual and Automatic Segmentation

A 3D model of the manual segmentation for the AMY, HC, PRC, ERC, and PHC is shown in **Figure 1**, and a sagittal section of the segmentation is shown in **Figure 2**. For the purpose of illustrating extreme possible differences between manual and automatic tracings, slices of the AMY from a representative subject with erroneous automated segmentation were juxtaposed with manual tracing (see **Figure 3** below). While automatic segmentation software was able to recognize the core body of the structures, its segmentation was rather rough, which resulted in underestimation of the AMY volume, compared to manual segmentation.

For illustration purposes, the results of manual tracing in one subject were compared with those obtained from automatic segmentation using an automatic segmentation program<sup>41-44</sup>; the focus was on the AMY and the HC. The AMY and HC volumes traced by the two methods were also corrected for the intracranial volume (ICV) of the subject (**Table 1**), using the following two steps: 1) The volumetric statistics of the AMY and HC segmentations: the manual segmentation software automatically calculated the volume statistics for labeled areas. This information was retrieved in "Volume and statistics" in the Segmentation menu when the to-be-examined segmentation along with its greyscale image was input into the software. 2) ICV Calculation: This was accomplished in three steps, using three programs in a standard automatic segmentation software<sup>42</sup>. An extraction process was used to extract the brain volume from the original image, stripping off non-brain tissue such as the skull. A partial volume extraction process was used to separate cerebrospinal fluid (CSF), the grey matter, and the white matter. Finally, a statistics process was used to sum up the partial volumes to obtain the ICV for the subject.

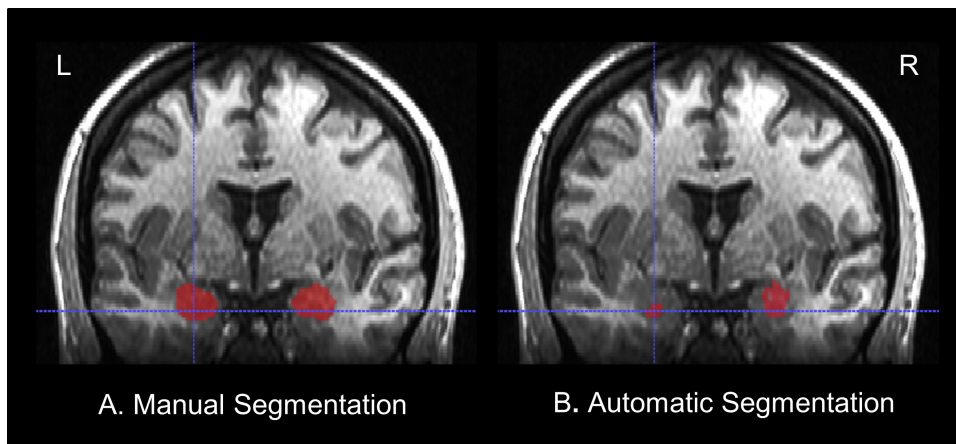


**Figure 3.** An extreme example of the possible differences between results of manual tracing (A) and automatic segmentation (B). Shown here is a coronal slice toward the anterior end of the AMY. As is evident from the comparison, automatic segmentation software has only recognized a small portion of the left AMY, while neglecting more than half of the tissue that is identifiable as part of the AMY to an expert human eye; similar underestimation, but to a lesser extent, also occurred in the right AMY.

Although **Figure 3** shows an example of extreme mismatch between manual and automated tracing, the possibility for misestimation of volume by automated segmentation still exists<sup>45</sup>. Such differences are illustrated in **Table 1** below, which compares the results of manual and automated tracing of the AMY and HC.

		Voxel volume (mm <sup>3</sup> )		Corrected volume	
		Manual	Auto	Manual	Auto
Amygdala	Left	1828.25	1506.75	0.11430	0.09420
	Right	1866.25	1494.75	0.11668	0.09345
Hippocampus	Left	4119.50	4493.50	0.25755	0.28093
	Right	4339.00	4513.50	0.27128	0.28219

**Table 1.** Representative volumetric results of the bilateral AMY and the HC of a single subject, from manual tracing using the present protocol and automatic segmentation. Automatic segmentation has misestimated the volume of each of the four structures compared. Corrected volume was calculated as the ratio between Voxel volume and ICV. For this subject, ICV = 1599482.11 mm<sup>3</sup>.

From these results, it is clear that automatic segmentation software may be capable of providing a reasonable localization of the MTL structures, but that the outcome of its segmentation can be further modified and refined through manual adjustments to meet a higher level of precision.

## Discussion

Traditionally, manual segmentation has been considered the gold standard by many researchers. Nevertheless, a precise delineation of the individual structures has been complicated by the highly variable morphology of the MTL structures, and by the usually weak MRI contrasts of these structures against the surrounding neural tissue and non-neural areas. Historically, there have been conflicting descriptions in the literature for some MTL structures. In some cases of segmenting the PRC, for example, the collateral sulcus has been described as interrupted<sup>35,36</sup>, but this has previously been described in other literature as a short CS which does not exceed the level of the limen insulae<sup>30</sup>. This difference in interpretation has led to different anterior border definitions for the PRC, and this might explain to some extent why variations have been observed in segmentations of individual structures across different studies. This is an aspect of segmentation where manual tracing can provide unique benefits, because visual examination allows for adaptation, which is difficult to implement in automatic segmentation. This can also be illustrated by the criteria used in the current protocol to delineate the PRC and the ERC. Of note, however, some researchers have suggested to always define the medial border of the PRC as the midpoint of the medial bank of the CS, regardless of sulcus depth<sup>30</sup>. Regarding the posterior PHC, due to the sometimes ambiguous boundary of the posterior PHC border, several definitions are described in the extant literature. In the current protocol, the boundary beyond the termination of the HC tail is used to reflect the common practice of measuring the PHC past the HC in both anatomical<sup>32</sup> and functional research<sup>46</sup>. However, the posterior PHC border has also been defined as being located more anteriorly, as 1.5 mm posterior to the crus of the fornix<sup>37</sup> and as the last slice in which the HC is located inferomedially to the trigone of the lateral ventricle<sup>30</sup>.

Depending on the purpose of the ROI and the resolution of the image, researchers might choose to include or exclude white matter in the segmentation. For example, inclusion of white matter might be appropriate for ROI use in fMRI, due to typical lower resolutions of the functional relative to anatomical scans. An example of this is offered by a previous study<sup>1</sup>, which shows a MTL slice with a 4 x 4 mm grid overlay (a typical fMRI resolution) where separating white matter and grey matter would be impossible. In anatomical research, however, a white matter/grey matter separation is usually performed, but even in anatomical research it is sometimes easier to delineate the borders if the structures are traced contiguously, which can lead to the inclusion of some white matter. If exclusion of white matter is preferred, tracing within the boundaries, rather than on them, can adjust the segmentation to avoid white matter volume.

The goal of the current protocol is to illustrate tracing guidelines in one participant, but in implementing a segmentation protocol for research purposes, reliability assessments should be calculated in order to verify that tracings are consistent within and across tracers. Depending on the goal of the study, there are several models that can be used to determine inter- and intra-rater reliability<sup>47</sup> for manual segmentation tracings. For comparisons between methods, intraclass correlation coefficients should be assessed<sup>48</sup>.

The benefit of manual segmentation of MR imaging data is the potential for increased accuracy and adaptability allowed by the flexibility in tracing and/or making adjustments based on knowledge of anatomy implemented in comprehensive guidelines. This flexibility can complement automatic tracing. Additionally, the use of MR imaging of *in vivo* brains such as in the current example allows for some methodological benefits such as longitudinal study, which might not be possible in other approaches (e.g., *post mortem*<sup>49</sup>). Although it can be difficult to translate cytoarchitecture to MR images, as acknowledged in a recent paper<sup>37</sup>, the use of notable landmarks can provide contextual guidelines that are usable across subjects. In segmenting the whole MTL, a tracer is given context and familiarity with surrounding structures which allows a level of adaptability and flexibility that can increase tracing accuracy. As we outline in our protocol, there are inconsistencies in the extant literature regarding the boundaries of MTL structures. Manual segmentation allows flexibility in implementing tracing guidelines, which is not as easily attainable by automatic segmentation algorithms. Additionally, the advantage of having working knowledge of relevant anatomical landmarks is also relevant if automatic segmentation fails, so that corrective measures can be taken based on good understanding of tracing guidelines regarding the borders of MTL (sub)regions, as described in our protocol.

Although speed and efficiency increase with training, a practical limitation of manual segmentation of brain structures is that it requires additional expertise in brain anatomy and a substantial devotion of time and effort. Hence, in the pursuit of higher efficiency, automated segmentation programs are also employed alternatively for the ROI segmentation. However, as the results of manual and automatic segmentation in the MTL illustrated here, the probabilistic estimation employed by automatic segmentation software can be less exact than manual approximation in these brain regions. The standard software used in the current protocol is one of several common options<sup>45</sup>, but the potential advantages and disadvantages of manual segmentation compared to automatic segmentation are similar regardless of the software chosen for automatic segmentation.

Overall, our view is that manual and automatic segmentation can be used as complementary methods. We suggest that automatic tracing results be checked and manually refined, if necessary, by expert tracers. The present protocol provides a set of guidelines for manual tracing of the MTL structures on high-resolution MR images. By taking advantage of the finer resolution of the current images, structures and landmarks can be accurately captured, so that the guidelines presented here can be applied to images of a wide range of resolutions. Along with the accompanying visual materials, this work is expected to provide and promote a clearer understanding of the gross anatomy of the MTL structures, and to encourage adoption of manual segmentation, either as the main method of MTL segmentation or as a complementary method to automatic segmentation.

## Disclosures

The authors have no conflicts of interest to declare.

## Acknowledgements

This research was supported by funds to FD. MM was supported by an IGERT Fellowship under National Science Foundation Grant No. 0903622. The authors wish to thank the Dolcos Lab members for assistance with data collection and preparation.

## References

1. Amaral, D. G. Introduction: what is where in the medial temporal lobe? *Hippocampus*. **9** (1), 1-6, doi:10.1002/(SICI)1098-1063(1999)9:1<1::AID-HIPO1>3.0.CO;2-T (1999).
2. Squire, L. R., & Zola-Morgan, S. The medial temporal lobe memory system. *Science*. **253** (5026), 1380-1386, doi:10.1126/science.1896849 (1991).
3. Eichenbaum, H., Otto, T., & Cohen, N. J. The hippocampus: what does it do? *Behavioral & Neural Biology*. **57** (1), 2-36, doi:10.1016/0163-1047(92)90724-I (1992).
4. Henke, K., Buck, A., Weber, B., & Wieser, H. G. Human hippocampus establishes associations in memory. *Hippocampus*. **7** (3), 249-256, doi:10.1002/(SICI)1098-1063(1997)7:3<249::AID-HIPO1>3.0.CO;2-G (1997).
5. Tulving, E., & Markowitsch, H. J. Episodic and declarative memory: role of the hippocampus. *Hippocampus*. **8** (3), 198-204, doi:10.1002/(SICI)1098-1063(1998)8:3<198::AID-HIPO2>3.0.CO;2-G (1998).
6. Dolcos, F., Iordan, A. D., & Dolcos, S. Neural correlates of emotion-cognition interactions: a review of evidence from brain imaging investigations. *Journal of Cognitive Psychology*. **23** (6), 669-694, doi:10.1080/20445911.2011.594433 (2011).
7. Davidson, R. J., & Irwin, W. The functional neuroanatomy of emotion and affective style. *Trends in Cognitive Sciences*. **3** (1), 11-21, doi:10.1016/S1364-6613(98)01265-0 (1999).
8. Lindquist, K. A., Wager, T. D., Kober, H., Bliss-Moreau, E., & Barrett, L. F. The brain basis of emotion: a meta-analytic review. *The Behavioral and Brain Sciences*. **35** (3), 121-143, doi:10.1017/S0140525X11000446 (2012).
9. Phan, K. L., Wager, T., Taylor, S. F., & Liberzon, I. Functional neuroanatomy of emotion: a meta-analysis of emotion activation studies in PET and fMRI. *Neuroimage*. **16** (2), 331-348, doi:10.1006/nimg.2002.1087 (2002).
10. Wager, T. D., Phan, K. L., Liberzon, I., & Taylor, S. F. Valence, gender, and lateralization of functional brain anatomy in emotion: a meta-analysis of findings from neuroimaging. *Neuroimage*. **19** (3), 513-31, doi:10.1016/S1053-8119(03)00078-8 (2003).
11. Zald, D. H. The human amygdala and the emotional evaluation of sensory stimuli. *Brain Research Reviews*. **41** (1), 88-123, doi:10.1016/S0165-0173(02)00248-5 (2003).
12. DeYoung, C. G., Hirsh, J. B., Shane, M. S., Papademetris, X., Rajeevan, N., & Gray, J. R. Testing predictions from personality neuroscience: brain structure and the big five. *Psychological Science*. **21** (6), 820-828, doi:10.1177/0956797610370159 (2010).
13. Visser, P. J., Verhey, F. R., Hofman, P. A., Scheltens, P., & Jolles, J. Medial temporal lobe atrophy predicts Alzheimer's disease in patients with minor cognitive impairment. *Journal of Neurology, Neurosurgery, & Psychiatry*. **72** (4), 491-497, doi:10.1136/jnnp.72.4.491 (2002).
14. Ezekiel, F. *et al.* Comparisons between global and focal brain atrophy rates in normal aging and Alzheimer disease. *Alzheimer Disease & Associated Disorders*. **18** (4), 196-201 (2004).
15. de Leon, M. J. *et al.* Imaging and CSF studies in the preclinical diagnosis of Alzheimer's disease. *Annals of the New York Academy of Sciences*. **1097**, 114-145, doi:10.1196/annals.1379.012 (2007).
16. Boccardi, M. *et al.* Survey of protocols for the manual segmentation of the hippocampus: preparatory steps towards a joint EADC-ADNI harmonized protocol. *Journal of Alzheimer's Disease*. **26** (Supplement 3), 61-75, doi:10.3233/JAD-2011-0004 (2011).
17. Konrad, C., Ukas, T., Nebel, C., Arolt, V., Toga, A. W., & Narr, K. L. Defining the human hippocampus in cerebral magnetic resonance images-an overview of current segmentation protocols. *Neuroimage*. **47** (4), 1185-1195, doi:10.1016/j.neuroimage.2009.05.019 (2009).
18. Hasboun, D. *et al.* MR determination of hippocampal volume: comparison of three methods. *American Journal of Neuroradiology*. **17** (6), 1091-1098 (1996).
19. Pantel, J. *et al.* A new method for the *in vivo* volumetric measurement of the human hippocampus with high neuroanatomical accuracy. *Hippocampus*. **10** (6) 752-758, doi:10.1002/1098-1063(2000)10:6<752::AID-HIPO1012>3.0.CO;2-Y (2000).
20. Entis, J. J., Doerga, P., Barrett, L. F., & Dickerson, B. C. A reliable protocol for the manual segmentation of the human amygdala and its subregions using ultra-high resolution MRI. *Neuroimage*. **60** (2), 1226-1235, doi:10.1016/j.neuroimage.2011.12.073 (2012).
21. Goncharova, I. I., Dickerson, B. C., Stoub, T. R., & deToledo-Morrell, L. MRI of human entorhinal cortex: a reliable protocol for volumetric measurement. *Neurobiology of Aging*. **22** (5), 737-745, doi:10.1016/S0197-4580(01)00270-6 (2001).
22. Watson, C. *et al.* Anatomic basis of amygdaloid and hippocampal volume measurement by magnetic resonance imaging. *Neurology*. **42** (9), 1743-1750, doi:10.1212/wnl.42.9.1743 (1992).
23. Duvernoy, H. *The human hippocampus: functional anatomy, vascularization, and serial sections with MRI*. Third Edition, (Springer-Verlag Berlin Heidelberg, 2005).
24. Amaral, D. G., & Witter, M. P. The three-dimensional organization of the hippocampal formation: a review of anatomical data. *Neuroscience*. **31** (3), 571-591, doi:10.1016/0306-4522(89)90424-7 (1989).
25. Insausti, R. *et al.* MR volumetric analysis of the human entorhinal, perirhinal, and temporopolar cortices. *American Journal of Neuroradiology*. **19** (4), 659-671 (1998).
26. Dolcos, F., LaBar, K. S., & Cabeza, R. Interaction between the amygdala and the medial temporal lobe memory system predicts better memory for emotional events. *Neuron*. **42** (5), 855-863, doi:10.1016/S0896-6273(04)00289-2 (2004).
27. Yushkevich, P. A. *et al.* User-guided 3D active contour segmentation of anatomical structures: significantly improved efficiency and reliability. *Neuroimage*. **31** (3), 1116-1128, doi:10.1016/j.neuroimage.2006.01.015 (2006).
28. Bonilha, L., Kobayashi, E., Cendes, F., & Li, M. L. Protocol for volumetric segmentation of medial temporal structures using high-resolution 3-D magnetic resonance imaging. *Human Brain Mapping*. **22** (2), 145-154, doi:10.1002/hbm.20023 (2004).
29. Bronen, R. A., & Cheung, G. Relationship of hippocampus and amygdala to coronal MRI landmarks. *Magnetic Resonance Imaging*. **9** (3), 449-457, doi:10.1016/0730-725X(91)90434-N (1991).
30. Pruessner, J. C. *et al.* Volumetry of temporopolar, perirhinal, entorhinal and parahippocampal cortex from high-resolution MR images: considering the variability of the collateral sulcus. *Cerebral Cortex*. **12** (12), 1342-1353, doi:10.1093/cercor/12.12.1342 (2002).
31. Pruessner, J. C. *et al.* Volumetry of hippocampus and amygdala with high-resolution MRI and three-dimensional analysis software: minimizing the discrepancies between laboratories. *Cerebral Cortex*. **10** (4), 433-442, doi:10.1093/cercor/10.4.433 (2000).
32. Duvernoy, H. *The human brain: surface, three-dimensional sectional anatomy with MRI, and blood supply*. Second Edition, (Springer-Verlag Wien, 1999).

33. Amaral, D. G., & Lavenex, P. in *The hippocampus book*. (eds P. Andersen *et al.*) Ch. Hippocampal neuroanatomy, (Oxford University Press, 2006).
34. Blaizot, X. *et al.* The human parahippocampal region: I. temporal pole cytoarchitectonic and MRI correlation. *Cerebral Cortex*. **20** (9), 2198-2212, doi:10.1093/cercor/bhp289 (2010).
35. Ding, S.-L., & Van Hoesen, G. W. Borders, extent, and topography of human perirhinal cortex as revealed using multiple modern neuroanatomical and pathological markers. *Human Brain Mapping*. **31** (9), 1359-1379, doi:10.1002/hbm.20940 (2010).
36. Ding, S.-L., Van Hoesen, G. W., Cassell, M. D., & Poremba, A. Parcellation of human temporal polar cortex: a combined analysis of multiple cytoarchitectonic, chemoarchitectonic, and pathological markers. *The Journal of Comparative Neurology*. **514** (6), 595-623, doi:10.1002/cne.22053 (2009).
37. Frankó, E., Insausti, A. M., Artacho-Pérula, E., Insausti, R., & Chavoix, C. Identification of the human medial temporal lobe regions on magnetic resonance images. *Human Brain Mapping*. **35** (1), 248-56, doi:10.1002/hbm.22170 (2014).
38. Lehmann, M. *et al.* Atrophy patterns in Alzheimer's disease and semantic dementia: a comparison of FreeSurfer and manual volumetric measurements. *Neuroimage*. **49** (3), 2264-2274, doi:10.1016/j.neuroimage.2009.10.056 (2010).
39. Winterburn, J. L. *et al.* A novel *in vivo* atlas of human hippocampal subfields using high-resolution 3T magnetic resonance imaging. *Neuroimage*. **74**, 254-265, doi:10.1016/j.neuroimage.2013.02.003 (2013).
40. Malykhin, N. V., Bouchar, T. P., Ogilvie, C. J., Coupland, N. J., Seres, P., & Camicioli, R. Three-dimensional volumetric analysis and reconstruction of amygdala and hippocampal head, body and tail. *Psychiatry research. Neuroimaging*. **155** (2), 155-165, doi:10.1016/j.psychres.2006.11.011 (2007).
41. Patenaude, B., Smith, S. M., Kennedy, D. N., & Jenkinson, M. A Bayesian model of shape and appearance for subcortical brain segmentation. *Neuroimage*. **56** (3), 907-922, doi:10.1016/j.neuroimage.2011.02.046 (2011).
42. Smith, S. M. *et al.* Advances in functional and structural MR image analysis and implementation as FSL. *Neuroimage*. **23** (Supplement 1), S208-S219, doi:10.1016/j.neuroimage.2004.07.051 (2004).
43. Woolrich, M. W. *et al.* Bayesian analysis of neuroimaging data in FSL. *Neuroimage*. **45** (1, Supplement 1), S173-S186, doi:10.1016/j.neuroimage.2008.10.055 (2009).
44. Smith, S. M. Fast robust automated brain extraction. *Human Brain Mapping*. **17** (3), 143-55, doi:10.1002/hbm.10062 (2002).
45. Morey, R. A. *et al.* A comparison of automated segmentation and manual tracing for quantifying hippocampal and amygdala volumes. *Neuroimage*. **45** (3), 855-866, doi:10.1016/j.neuroimage.2008.12.033 (2009).
46. Baldassano, C., Beck, D. M., & Fei-Fei, L. Differential connectivity within the parahippocampal place area. *Neuroimage*. **75**, 228-37, doi:10.1016/j.neuroimage.2013.02.073 (2013).
47. Shrout, P. E., & Fleiss, J. L. Intraclass correlations: uses in assessing rater reliability. *Psychological Bulletin*. **86** (2), 420-428, doi:10.1037/0033-2909.86.2.420 (1979).
48. Bland, J. M., & Altman, D. G. A note on the use of the intraclass correlation coefficient in the evaluation of agreement between two methods of measurement. *Computers in Biology and Medicine*. **20** (5), 337-340, doi:10.1016/0010-4825(90)90013-F (1990).
49. Yushkevich, P. A. *et al.* A high-resolution computational atlas of the human hippocampus from postmortem magnetic resonance imaging at 9.4 T. *Neuroimage*. **44** (2), 385-398, doi:10.1016/j.neuroimage.2008.08.042 (2009).